Journal of the Brazilian Society of Mechanical Sciences and Engineering (2024) 46:181
https://doi.org/10.1007/s40430-024-04762-9

TECHNICAL PAPER

A two-layer description for some benchmark turbulent flows applicable to arbitrary values of the Reynolds number and the wall roughness

Seyed Reza Saleh[1] · **Iman Zahmatkesh**[1]

Received: 31 August 2023 / Accepted: 5 February 2024 / Published online: 7 March 2024

Abstract

According to the existing theory, turbulent flow fields are divided into four layers, including (a) the viscous sublayer, (b) the buffer layer, (c) the logarithmic layer, and (d) the core layer. However, in this work, a two-layer description for some benchmark turbulent flows is proposed. To arrive at this description, firstly, the logarithmic layer is extended to include the buffer layer, which removes the need to consider the buffer layer with its complex formula. Thereafter, the attention is focused on some benchmark problems in fluid mechanics (i.e., the Couette flow, the 2D channel flow, the circular pipe flow, and the flow over a flat plate) and new descriptions are proposed for their core layers, incorporating the extended logarithmic layer. Hence, the accomplished two-layer description divides the considered turbulent flows into only (a) the viscous sublayer and (b) the extended core layer, each with a corresponding velocity profile. This description substantially simplifies the analysis and can be helpful for future studies. The proposed description is applicable to smooth as well as rough walls and is accurate for low, intermediate, and high Reynolds numbers. It is found that in spite of the simplicity of the proposed two-layer description, its outcomes in terms of the time-averaged velocity profile are in excellent agreement with those of previous studies, for all of the considered benchmark problems.

Keywords Turbulent flow · Surface roughness · Viscous sublayer · Buffer layer · Logarithmic layer

List of symbols

A	Constant coefficient defined in Eq. (32)
B	Constant coefficient defined in Eq. (32)
C	Constant coefficient defined in Eq. (32)
$\overline{C}$	Constant coefficient defined in Eq. (28)
D	Constant coefficient defined in Eq. (32)
K_s	Equivalent sand roughness
K_{tech}	Technical roughness
K_s^+	Dimensionless value of the equivalent sand roughness, $K_s^+ = K_s u_\tau/\upsilon$
K_{tech}^+	Dimensionless value of the technical roughness,$K_{tech}^+ = K_{tech} u_\tau/\upsilon$
h	Half of the distance between the plates
L_r	Reference length, $L_r = h$, R, or δ
r	Radial direction
R	Pipe radius
Re	Reynolds number
Re_{crit}	Critical Reynolds number
Re_d	Reynolds number based on the pipe diameter, $Re_d = 2\overline{u}_m R/\upsilon$
Re_x	Reynolds number based on the distance from the leading edge, $Re_x = u_\infty x/\upsilon$
Re_τ	Reynolds number based on the friction velocity, $Re_\tau = u_\tau L_r/\upsilon$
$Re_{\tau,crit}$	Critical Reynolds number based on the friction velocity
u_{mean}	Mean velocity
u_τ	Friction velocity, $u_\tau = \sqrt{\overline{\tau}_w/\rho}$
u^+	Dimensionless velocity, $u^+ = \overline{u}/u_\tau$
u_c^+	Dimensionless velocity at the centerline, $u_c^+ = u^+(\eta = 0)$
u_l^+	Dimensionless velocity at the start of the extended logarithmic layer, $u_l^+ = u^+\left(y_l^+\right)$

Technical Editor: Daniel Onofre de Almeida Cruz.

✉ Iman Zahmatkesh
zahmatkesh5310@mshdiau.ac.ir;
iman.zahmatkesh@gmail.com

Seyed Reza Saleh
r-saleh@mshdiau.ac.ir; saleh@mshdiau.ac.ir

[1] Department of Mechanical Engineering, Mashhad Branch, Islamic Azad University, Mashhad, Iran

u^+_{wall} Dimensionless velocity of the wall for the Couette flow, $u^+_{wall} = 2u^+_c$
U_∞ Free stream velocity
$\overline{u}$ Time-averaged velocity
y Vertical distance from the wall
y^+ Characteristic wall coordinate, $y^+ = Re_\tau(1-\eta)$
y^+_l Starting point of the extended logarithmic layer from the wall
z Parameter defined as $z = \eta/\eta_l$

Greek symbol

δ Thickness of the hydrodynamic boundary layer
ε Constant coefficient defined in Eq. (32)
η Dimensionless distance from the centerline, $\eta = (yorr)/L_r$
η_l Starting point of the extended logarithmic layer from the centerline, $\eta_l = 1 - y^+_l/Re_\tau$
κ Karman constant
μ Dynamic viscosity
μ_t Turbulent dynamic viscosity
ρ Fluid density
τ_t Turbulent shear stress in a turbulent flow
τ_{total} Total shear stress in a turbulent flow
$\overline{\tau}_w$ Time-averaged shear stress at the wall
υ Kinematic viscosity
υ_t Turbulent kinematic viscosity

1 Introduction

Due to the nonlinearity of the Navier–Stokes equations, analytic solutions of these equations are hard to achieve. Hence, only a limited number of such solutions are available in the literature. For instance, Saleh and Rahimi [1] accomplished an exact solution for unsteady axisymmetric stagnation-point flow over a moving cylinder subjected to transpiration. Ghiasi and Saleh [2] presented an analytic solution for unsteady MHD flow over a shrinking horizontal sheet. Housiadas and Georgiou [3] derived an analytical solution for the flow of a fluid having pressure-dependent viscosity through a rectangular duct. Kannaiyan et al. [4] presented an analytic solution for unsteady pipe flows. Akhtar and Shah [5] obtained analytic solutions for Couette flow, Generalized Couette flow, and Poiseuille flow, under unsteady conditions. Moreover, Nec and Huculak [6] presented an analytic solution for radial flow in a porous medium having non-uniform permeability. Some of the analytic solutions have been collected in the books of Schlichting and Gersten [7] and White [8].

Compared to the laminar flow fields, accomplishing an analytic solution for the Navier–Stokes equations in turbulent flows is inherently more complex which goes back to the existence of the irregular fluctuations in the flow properties therein. These fluctuations can be omitted through the time-averaging procedure. But, this is accompanied by the appearance of some new terms, which are called the Reynolds (turbulent) stresses that need to be approximated through turbulence models. Going into the literature indicates that analytic solutions of turbulent flows are usually limited to simple geometries. For instance, García and Alvariño [9] offered an analytic solution for turbulent pipe flows under unsteady conditions. In another attempt, an analytic solution for a partially-submerged pipe with the attendance of reciprocating flow was presented by Hasan et al. [10].

The topic of universality of wall-bounded flows has been discussed for many decades. However, the recent study of Heinz [11] demonstrates that the structure of such flow fields is much more universal than previously expected. To analysis a wall-bounded flow, the flow field is divided into four layers, namely, the viscous sublayer, the buffer layer, the logarithmic layer, and the core layer. In such a four-layer description, each layer is solved separately, while solutions of the adjacent layers are matched. A glance at the recent review paper of Kadivar et al. [12] shows that this four-layer description for turbulent flows has not been changed considerably for many years.

In the present paper, firstly, the shortcomings of the existing theory for the near-wall layer as well as the core layer are presented. Thereafter, the logarithmic layer is extended to include the buffer layer, which removes the need to consider the buffer layer with its complex formula. Finally, some benchmark problems in fluid mechanics including the fully-developed Couette flow, the fully-developed 2D channel flow, the fully-developed circular pipe flow, and flow over a flat plate are considered and new descriptions are proposed for their core layers, incorporating the extended logarithmic layer. Hence, the proposed description divides the turbulent flow field into only the viscous sublayer and the extended core layer. This provides substantial simplification in the analysis, compared with the existing theory, which divides the flow field into four layers. The accomplished description is valid for small, medium, and large Reynolds numbers as well as smooth and rough walls.

The considered benchmark problems, in spite of their geometrical simplicity, have been a matter of constant study, due to their practical applications. Recently, Teja et al. [13] discussed the onset of shear-layer instability at the interface of parallel Couette flows. Ohta et al. [14] analyzed the modulation of turbulent Couette flow with vortex cavitation in a minimal flow unit. Hasanuzzaman et al. [15] discussed the enhanced outer peaks in turbulent boundary layer using uniform blowing. Jiao et al. [16] studied how the adverse pressure gradient may alter the near-wall turbulence in the Couette flow. Ilter [17] simulated the fully developed channel flow over a dimpled surface in the turbulent flow regime. Meanwhile,

the consequences of the wall roughness have attracted the attention of many researchers. In a recent attempt, Mangavelli et al. [18] analyzed the effect of surface roughness topography on unsteady channel flows. Kracik and Dvorak [19] discussed how the wall roughness may affect the secondary flow choking in an air ejector. Li et al. [20] proposed a model for the prediction of the turbulent boundary layer downstream of a step-change in the wall roughness. Sorgun et al. [21] analyzed the turbulent flows of Herschel-Bulkley and power-law fluids in rough pipes. Aghaei-Jouybari et al. [22] paid attention to the fully developed supersonic flow over sinusoidal rough walls in the turbulent flow regime. Hosseinzade and Berstrom [23] proposed a wall stress model for the analysis of turbulent flows over rough walls. Moreover, thanks to a four-layer description for the mixing length function, She et al. [24] presented a Lie-group symmetry analysis to arrive at analytical expressions for the mean-velocity profile in the fully-developed 2D channel flow, the fully-developed circular pipe flow, and flow over a flat plate.

2 Basic equations

In a turbulent flow field, the shear stress is composed of two parts: (a) the stress generated by the fluid viscosity (b) the stress generated by the flow turbulence. Hence, the total shear stress in a turbulent flow is frequently written as [7]:

$$\tau_{\text{total}}(y) = \mu \frac{\mathrm{d}\overline{u}}{\mathrm{d}y} + \mu_t \frac{\mathrm{d}\overline{u}}{\mathrm{d}y} = \left(\mu + \mu_t\right) \frac{\mathrm{d}\overline{u}}{\mathrm{d}y} \tag{1}$$

To provide a universal description for the analysis, we define η as the dimensionless distance from the centerline or the boundary layer edge. The values of this parameter for the current flow problems are introduced in Table 1. With this definition, Eq. (1) takes the following form:

$$\tau_{\text{total}}(\eta) = -\frac{\rho\left(\upsilon + \upsilon_t\right)}{L_r} \frac{\mathrm{d}\overline{u}}{\mathrm{d}\eta} \tag{2}$$

Rearrangement of Eq. (2) leads to:

Table 1 The values of η for the current benchmark problems

Flow problem	η	L_r
The Couette flow	$\eta = 1 - \frac{y}{L_r}$	h
2D channel flow	$\eta = 1 - \frac{y}{L_r}$	h
Pipe flow	$\eta = 1 - \frac{y}{L_r} = \frac{r}{L_r}$	R
Flow over a flat plate	$\eta = 1 - \frac{y}{L_r}$	δ

$$\frac{\mathrm{d}\overline{u}}{\mathrm{d}\eta} = -\frac{1}{1 + \frac{\upsilon_t}{\upsilon}} \frac{\overline{\tau}_w}{\rho} \frac{L_r}{\upsilon} \frac{\tau_{\text{total}}(\eta)}{\overline{\tau}_w} \tag{3}$$

Adopting the friction velocity, $u_\tau = \sqrt{\overline{\tau}_w/\rho}$, the above equation can expressed in terms of the dimensionless velocity, $u^+ = \overline{u}/u_\tau$, and the Reynolds number, $Re_\tau = u_\tau L_r/\upsilon$, as:

$$\frac{\mathrm{d}u^+}{\mathrm{d}\eta} = -\frac{\mathrm{Re}_\tau}{1 + \frac{\upsilon_t}{\upsilon}(\eta)} \frac{\tau_{\text{total}}(\eta)}{\overline{\tau}_w} \tag{4}$$

The above relation is exact and is applicable to the entire flow field. However, some improper use of this relation has been occurred, which reduced the accuracy of the existing theory. These shortcomings are discussed in the following sections.

3 Shortcomings of the existing theory for the near-wall layer

For a better depiction of the velocity slope in the vicinity of the wall, we define the characteristic wall coordinate as $y^+ = Re_\tau(1 - \eta)$. With this definition, Eq. (4) takes the following form for the near-wall layer:

$$\frac{\mathrm{d}u^+}{\mathrm{d}y^+} = \frac{1}{1 + \frac{\upsilon_t}{\upsilon}(y^+)} \frac{\tau_{\text{total}}\left(y^+\right)}{\overline{\tau}_w} \tag{5}$$

The shear stress in a turbulent flow, $\tau_{total}(\eta)$, is equal to $\overline{\tau}_w$ for the Couette flow and $\overline{\tau}_w\eta$ for the 2D channel flow, the circular pipe flow, and flow over a flat plate [7]. It is noteworthy that for the flow over a flat plate, the approximate von Karman profile [25] is utilized to arrive at this result. Hence, in the Couette flow, one has:

$$\frac{\tau_{\text{total}}\left(y^+\right)}{\overline{\tau}_w} = 1 \tag{6}$$

Meanwhile, for the other benchmark problems selected here, we can write:

$$\frac{\tau_{\text{total}}\left(y^+\right)}{\overline{\tau}_w} = \eta = 1 - \frac{y^+}{\mathrm{Re}_\tau} \tag{7}$$

However, in the near-wall layer, $y^+/Re_\tau \cong 0$. This reduces Eqs. (7)–(6), simplifying Eq. (5) as:

$$\frac{\mathrm{d}u^+}{\mathrm{d}y^+} = \frac{1}{1 + \frac{\upsilon_t}{\upsilon}(y^+)} \tag{8}$$

It should be noted that, if the attention be limited to the viscous sublayer, $\upsilon_t/\upsilon \cong 0$ reduces Eq. (8) to:

$$\frac{du^+}{dy^+} \cong 1 \tag{9}$$

which is a familiar relation for this layer.

Shortcoming # 1: The existing theory improperly assumes that in the logarithmic layer $\upsilon_t \gg \upsilon$. This reduces Eq. (8) to:

$$\frac{du^+}{dy^+} = \frac{1}{\frac{\upsilon_t}{\upsilon}(y^+)} \tag{10}$$

Although this assumption becomes reasonable at the high values of the Reynolds number or far from the wall, it produces some errors in the low values of the Reynolds number or in the vicinity of the wall. We will show later that avoiding this improper assumption extends the applicability of the logarithmic layer to the lower values of y^+.

Shortcoming # 2: The second shortcoming in the description of the near-wall layer goes back to the relation employed for the logarithmic layer. Indeed, in this layer, one has:

$$\lim_{y^+\to\infty} \frac{\upsilon_t}{\upsilon}\left(y^+\right) = \kappa y^+ \tag{11}$$

However, in the existing theory, the above relation has improperly been converted into the following form [7]:

$$\frac{\upsilon_t}{\upsilon}\left(y^+\right) = \kappa y^+ \tag{12}$$

with $\kappa = 0.41$.

This improper modification reduces the precision of the turbulence description in the low values of y^+ and necessitates to consider an additional layer (i.e., the buffer layer) to capture the flow field between the viscous sublayer and the logarithmic layer.

4 Shortcoming of the existing theory for the core layer

One may adopt Eq. (4) for the velocity slope in the core layer. Closer scrutiny of this relation shows that it is not exactly the same as the common relation utilized in the existing theory [7]. However, notice that if we assume that $\upsilon_t \gg \upsilon$ in the core layer, the denominator reduces to υ_t/υ and the existing relation for the core layer is recovered as:

$$\frac{du^+}{d\eta} = -\frac{\mathrm{Re}_\tau}{\frac{\upsilon_t}{\upsilon}(\eta)}\frac{\tau_{\mathrm{total}}(\eta)}{\overline{\tau}_w} \tag{13}$$

From the physical point of view, such an assumption may not hold in the low values of the Reynolds number or in the vicinity of the wall. It will be shown later that avoiding this improper assumption substantially enhances the range of applicability of Eq. (4).

5 The proposed two-layer description

When the Reynolds number is sufficiently large, the near-wall layer is not a large domain in comparison with the total flow field. Hence, the solution of the near-wall layer is independent to the flow geometry and thus a universal solution exists for this layer for all geometrical configurations. However, solution of the core layer is always strongly dependent to the geometry of the flow field, and this layer must be solved separately for each geometrical configuration.

In the following sections, firstly, the derivation of the velocity distribution in the viscous sublayer is reviewed in Sect. 5.1. Then, in Sect. 5.2, the logarithmic layer is extended to include the buffer layer, which removes the need to consider the buffer layer with its complex formula. In this section, the smooth walls provide a suitable circumstance to validate the proposed two-layer description. The presented materials are accompanied by calculating the starting point of the extended logarithmic layer in Sect. 5.3. Thereafter, the existing geometry-dependent solutions of the core layer are presented for the current benchmark problems in Sect. 5.4. It will be shown that the main drawback of these solutions is the fact that they lose their accuracy in the vicinity of the wall. To remove this shortcoming, in Sect. 5.5, a new variable is introduced for the dimensionless distance. Thanks to this variable, the extended core layer solutions are proposed for the current benchmark problems. These solutions incorporate the extended logarithmic layer too. Hence, we will arrive at a two-layer description for the current benchmark problems in this section. The proposed description is applicable to arbitrary values of the Reynolds number. Finally, in Sect. 5.6 this description is utilized to simulate the flow field in the current benchmark problems. In order to validate the proposed description further, the presented results are compared with those of the open literature.

5.1 The viscous sublayer

The viscous sublayer is a region of a turbulent flow that is close to a no-slip boundary and where viscous shear stresses play a significant role. The flow velocity decreases toward the no-slip boundary due to the no-slip condition, resulting in a region near the wall where the flow velocities are small. In this region, the viscous term is dominant, and the inertial terms in the Navier–Stokes equation are negligible. The roughness height relative to this sublayer has a significant impact on hydraulics. Flow is considered hydraulically rough if the roughness elements are larger than the laminar sublayer which perturbs the flow, and hydraulically smooth if they are smaller

than the laminar sublayer, which the main body of the flow ignores. Velocity distribution in the viscous sublayer is computed according to Eq. (9) as:

$$u^+ = y^+ \tag{14}$$

which is a generally accepted relation for this layer in the literature. However, it will be shown later (Sect. 5.3) that in the proposed description, the ending point of the viscous sublayer takes a longer distance from the wall.

5.2 The extended logarithmic layer

In the extended logarithmic layer (i.e., $y^+ > y_l^+$ with y_l^+ being the starting point of this layer), to remove Shortcoming # 2 in Sect. 3, instead of the existing equation for the dimensionless eddy viscosity in the form of $\upsilon_t/\upsilon = \kappa y^+$ (i.e., Equation (12)), the following relation is proposed:

$$\frac{\upsilon_t}{\upsilon} = \kappa\left(y^+ - y_l^+\right) \tag{15}$$

Notice that the proposed relation reduces to the existing relation for the logarithmic layer as $y^+ \to \infty$ and thereby, it automatically satisfies Eq. (11). Meanwhile, it is obvious that υ_t/υ vanishes at y_l^+. Hence, y_l^+ in Eq. (15) which is the starting point of extended logarithmic layer represents the thickness of the viscous sublayer. Indeed, this relation extends the logarithmic layer up to the viscous sublayer and excludes the need to incorporate the buffer layer as a distinct layer with its complex formula. The parameter y_l^+ for an arbitrary value of the wall roughness will be calculated later in Sect. 5.3. However, it will be shown there that for flow over a smooth wall, one has $y_l^+ = 7.2$. This indicates that the proposed relation (i.e., Eq. (15)) is distinct from the so-called "log-layer offset" concept which is utilized in most of the roughness models (Durbin [26], Ismail [27], and Squire et al. [28]). We will find in Sect. 5.2.2 that in the special case of rough walls, the proposed relation reproduces the log-layer offset concept.

To provide a picture about the suitability of Eq. (15), Fig. 1 is plotted. The figure indicates the variations of the near-wall values of the dimensionless eddy viscosity for different cases of the wall roughness. Notice that for flow over a smooth wall, provided that $y^+ \le y_l^+ = 7.2$, the viscous sublayer establishes with $\upsilon_t/\upsilon = 0$. However, for $y^+ > 7.2$, υ_t/υ varies according to $\upsilon_t/\upsilon = \kappa\left(y^+ - 7.2\right) \cong \kappa y^+ - 3$ representing the extended logarithmic layer. This can be expressed mathematically as:

$$\frac{\upsilon_t}{\upsilon} = \begin{cases} 0 & \text{for } y^+ \le 7.2 \\ \kappa y^+ - 3 & \text{for } y^+ \ge 7.2 \end{cases} \tag{16}$$

Closer scrutiny of Fig. 1 demonstrates that with increase in the wall roughness, y_l^+ decreases until the critical roughness wherein $y_l^+ = 0$. In this circumstance,

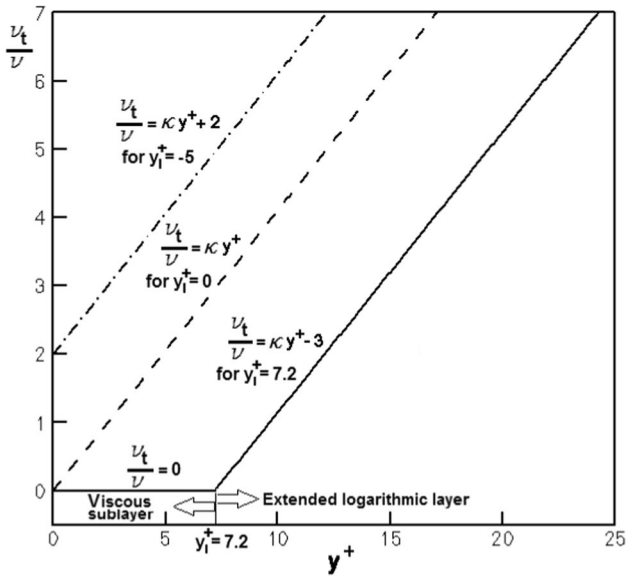

Fig. 1 The near-wall values of the dimensionless eddy viscosity for (a) The smooth wall having $y_l^+ = 7.2$, (b) The critical value of the wall roughness with $y_l^+ = 0$, (c) A typical case of the fully rough wall having $y_l^+ = -5$

the viscous sublayer disappears completely and υ_t/υ alters according to $\upsilon_t/\upsilon = \kappa y^+$. Here, the extended logarithmic layer initiates from the wall. Inspection of Fig. 1 also shows that passing the critical roughness (i.e., the fully rough wall) leads to $y_l^+ < 0$. Here, υ_t/υ is no longer zero at the wall in a way that rise in the wall roughness elevates the value of υ_t/υ at the wall. For instance, notice the case having $y_l^+ = -5$ and $\upsilon_t/\upsilon = \kappa\left(y^+ + 5\right) \cong \kappa y^+ + 2$. In this condition, again, the extended logarithmic layer initiates from the wall.

To remove Shortcoming # 1 in Sect. 3, instead of Eqs. (10), (8) is adopted for the velocity gradient in the extended logarithmic layer. Combining Eqs. (8) and (15) yields:

$$\frac{\mathrm{d}u^+}{\mathrm{d}y^+} = \frac{1}{1 + \kappa\left(y^+ - y_l^+\right)} \tag{17}$$

which takes the following form for flow over a smooth wall:

$$\frac{\mathrm{d}u^+}{\mathrm{d}y^+} = \frac{1}{1 + \kappa(y^+ - 7.2)} \cong \frac{1}{\kappa y^+ - 2} \tag{18}$$

After integrating Eq. (17), the following relation is obtained for the velocity distribution in the extended logarithmic layer:

$$u^+ = C^+ + \frac{1}{\kappa}\ln\left(y^+ - y_l^+ + \frac{1}{\kappa}\right) \tag{19}$$

5.2.1 Simplifying the analysis for the smooth walls

The deliberations until now belong to the general case having an arbitrary value of the wall roughness. However, the smooth walls provide a suitable circumstance to validate the proposed description. Hence, in this section the analysis is simplified to this special case. We will further discuss the general case in Sect. 5.2.2.

Figure 2 depicts the variation of the velocity gradient in the extended logarithmic layer (i.e., Eq. (18) for $y^+ > 7.2$) combined with the viscous sublayer (i.e. Equation (9) for $y^+ \le 7.2$). In this figure, the existing logarithmic layer with the form of $du^+/dy^+ = 1/\kappa y^+$ is also depicted for comparison. It is obvious that in the existing theory, the buffer layer needs to be included to capture the flow field between the viscous sublayer and logarithmic layer since the logarithmic layer loses its accuracy at the low values of y^+. This is in accord with the previous findings which limit the suitability of the logarithmic layer to $y^+ > 70$ [7].

It will be shown in Sect. 5.2.2 that for flow over a smooth wall, one has: $C^+ \cong 5$. Hence, Eq. (19) takes the following form for this circumstance:

$$u^+ = 5 + \frac{1}{\kappa}\ln\left(y^+ - 4.8\right) \cong 5 + \frac{1}{\kappa}\ln\left(y^+ - 5\right) \tag{20}$$

The above relation represents a more comprehensive relation than the existing one for the logarithmic layer of the smooth walls. Indeed, in the existing theory, the relation of $u^+ \cong 5 + 1/\kappa \ln y^+$ is adopted for the logarithmic layer (i.e., $y^+ \to \infty$) while a more complex correlation is utilized for the buffer layer. The following limit clearly demonstrates that the discrepancies appearing between the results of the extended logarithmic relation and those of the existing one are vanishing at far distances from the wall:

$$\lim_{y^+\to\infty}\left[5 + \frac{1}{\kappa}\ln\left(y^+ - 5\right)\right] = 5 + \frac{1}{\kappa}\ln y^+ \tag{21}$$

Equation (20) combined with Eq. (14) yields the velocity profile for flow over a smooth wall as:

$$u^+ = \begin{cases} y^+ & \text{for} y^+ \le 7.2 \\ 5 + \frac{1}{\kappa}\ln\left(y^+ - 5\right) & \text{for} y^+ \ge 7.2 \end{cases} \tag{22}$$

This relation is portrayed in Fig. 3. Here, results of the experimental evidences as well as the asymptotes at $y^+ \to 0$ (i.e., $u^+ = y^+$) and $y^+ \to \infty$ (i.e., $u^+ = 5 + \frac{1}{\kappa}\ln y^+$) are also provided for comparison. Notice that the results of the current description bear a strong resemblance with those of the experimental evidences. It is evident that the existing logarithmic layer losses its accuracy at $y^+ < 70$, necessitating to consider the buffer layer between the viscous sublayer and the logarithmic layer. However, notice that the extended logarithmic layer is accurate for $y^+ > 7.2$. Indeed, the relation proposed in this study can cover both layers well, indicating that there is no need to consider the buffer layer separately.

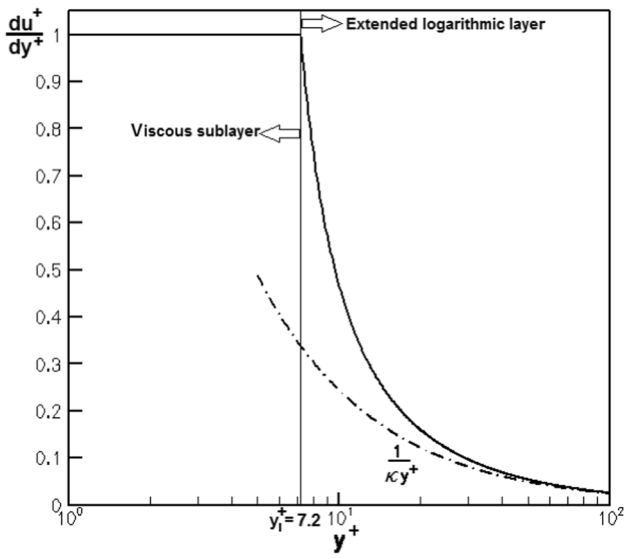

Fig. 2 The proposed near-wall velocity gradient for flow over a smooth wall including the viscous sublayer and the extended logarithmic layer compared with the existing logarithmic layer in the form of $du^+/dy^+ = 1/\kappa y^+$

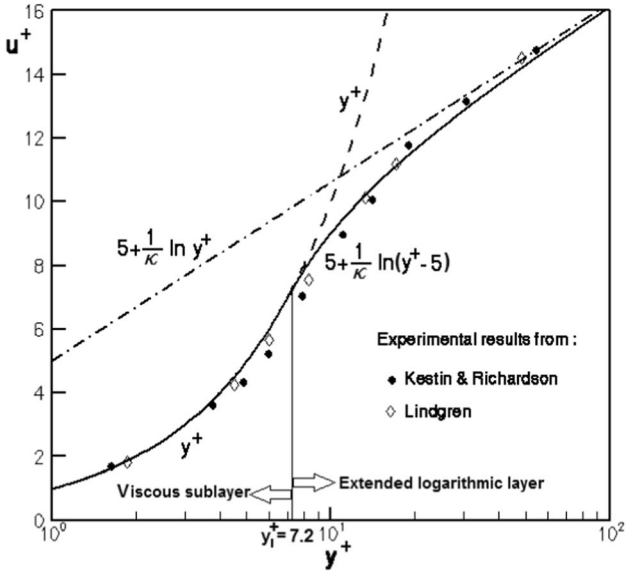

Fig. 3 The proposed near-wall velocity profile for flow over a smooth wall compared with the experimental results of Kestin and Richardson [35] and Lindgren from the book of White [25] as well as the asymptotes at $y^+ \to 0$ and $y^+ \to \infty$

With this description, the buffer layer becomes a part of this extended logarithmic layer while the starting point of the extended logarithmic layer instead of $y_l^+ \cong 70$ occurs at $y_l^+ = 7.2$, which is the edge of the viscous sublayer.

5.2.2 Analysis of arbitrary value of the wall roughness

In the previous, the smooth walls provided a suitable circumstance to validate our two-layer description. In what follows, attention is focused to the general case, having an arbitrary value of the wall roughness. This section will be helpful for practical applications wherein the walls exhibit some roughness.

According to the experimental results of Tani [29], the constant C^+ appearing in Eq. (19) is a function of the dimensionless wall roughness. Adopting curve fitting for these data, we propose the following relation for C^+ in terms of the dimensionless sand roughness $K_s^+ = K_s u_\tau/\upsilon$ with K_s being the sand roughness height:

$$C^+\left(K_s^+\right) = 8 - \frac{1}{\kappa}\ln\left[K_s^+ - 16\left(1 - e^{\frac{3.1-K_s^+}{16}}\right)\right] \tag{23}$$

The variations of C^+ with K_s^+ according to Eq. (23) in conjunction with the experimental data of Tani [29] are depicted in Fig. 4. Notice that the results of the proposed relation bear a strong resemblance to the experimental data. This demonstrates the suitability of the proposed relation for future studies of turbulent flows. Closer scrutiny of the figure shows that for a "perfectly smooth wall" ($K_s^+ = 0$), one has $C^+ = 5$. Then, C^+ slightly increases with increasing the sand roughness until $K_s^+ = 6$. Thereafter, it decreases again, reaching the value of 5. Therefore, this region is recognized as "the hydraulically smooth zone". With further rise in the sand roughness, C^+ decreases until the fully rough regime occuring at $K_s^+ > 80$ and $C^+ < -2.175$. It is evident that in the limiting case of $K_s^+ < 6$, Eq. (23) reduces to $C^+ \cong 5$ while in the limiting condition of "the fully rough regime" ($K_s^+ \to \infty$), one has $C^+ \cong 8 - 1/\kappa \ln K_s^+$. These limiting relations are in accord with the correlations presented in [29].

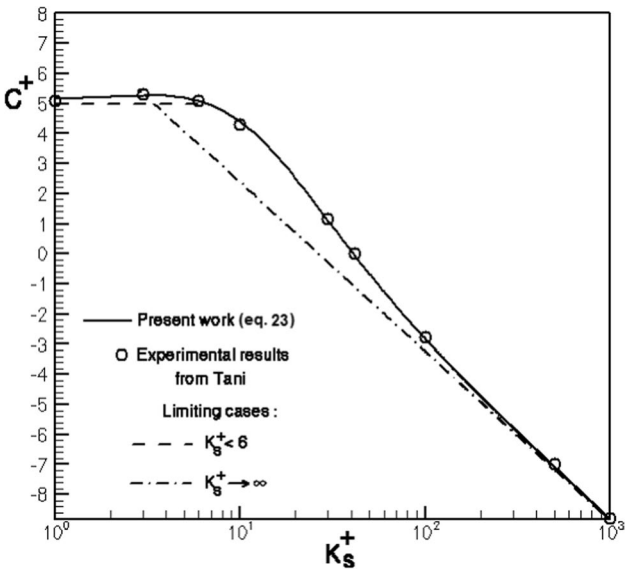

Fig. 4 Variations of C^+ with K_s^+ according to Eq. (23) compared with the experimental results of Tani [29] under two limiting cases of very low roughness (hydraulically smooth) and very high roughness (fully rough regime)

It is noteworthy that if instead of the dimensionless sand roughness, one adopts the dimensionless technical roughness, $K_{\text{tech}}^+ = K_{\text{tech}} u_\tau/\upsilon$, (with K_{tech} being the technical roughness height) the Colebrook's [30] relation should be employed as:

$$C^+\left(K_{\text{tech}}^+\right) = 8.0 - \frac{1}{\kappa}\ln\left(K_{\text{tech}}^+ + 3.4\right) \tag{24}$$

It should be noted that for the technical roughness, the fully rough regime occurs at $K_{\text{tech}}^+ > 60$, as suggested by Colebrook formula.

In the experimental evidences of McKeon et al. [31], the value of C^+ has been changed to 5.6. Meanwhile, the numbers of 8 and 3.4 in the Colebrook relation have been modified to 7.81 and 2.54, respectively [32]. However, since the above changes have not been applied in the text book by Schlichting and Gersten [7], these new constants have not been considered here. However, if one uses these modified constants, the constants appearing in Eq. (23) should also be modified.

The near-wall velocity profile depicted in Fig. 3 belonged to the special case of the flow over smooth walls. Now, we replace the proposed relation for C^+ (i.e., Eq. 23) in the relation of the extended logarithmic layer (i.e., Eq. 19) to arrive at the near-wall velocity profile corresponding to the general case having an arbitrary value of the wall roughness. Results for several values of the wall roughness are depicted in Fig. 5. Notice the alternation of the velocity profile due to the intensification of the wall roughness. The trend of the alternation is in accord with Schlichting [33].

5.3 Starting point of the extended logarithmic layer

The extent to which the extended logarithmic layer starts from the wall, y_l^+, is an important parameter which depends on C^+. The relation between these two parameters is as follows:

For the wall roughness values smaller than the critical roughness (i.e., $C^+ > -2.175$), the velocity at the starting point of the extended logarithmic layer in Eqs. (14) and (19) are matching in a way that $y_l^+ > 0$.

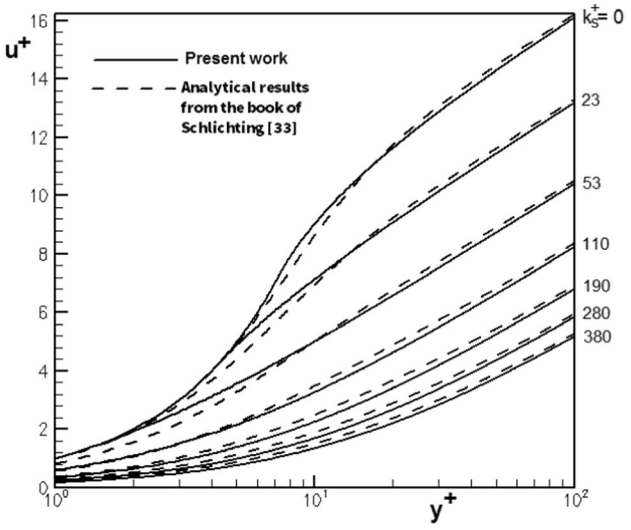

Fig. 5 The near-wall velocity profile for the general case having an arbitrary value of the wall roughness, compared with the analytical results [33]

Meanwhile, for the wall roughness values higher than the critical roughness (i.e., $C^+ < -2.175$), one has $y_l^+ < 0$. The negativity of the viscous sublayer thickness indicates that the wall roughness is so high allowing the flow to penetrate into the roughness cavities in a way that with the kinematic eddy viscosity is practically non-zero at $y^+ = 0$. In this case, the flow starts with the logarithmic layer and thereby, the viscous sublayer may not establish. Hence, the solution of the logarithmic layer remains true for all of the near-wall layer. This case is frequently termed as "the completely rough flow".

However, for $C^+ = -2.175$, one has $y_l^+ = 0$ indicating that the viscous sublayer is completely omitted. This value of C^+ represents the starting point of a fully rough flow and is called "the critical wall roughness".

Based on the above cases, we propose the following relation for y_l^+:

$$y_l^+ = \begin{cases} C^+ + \frac{1}{\kappa}\ln\frac{1}{\kappa} & \text{for } C^+ \geq -2.175 \\ \frac{1}{\kappa} - e^{-\kappa C^+} & \text{for } C^+ \leq -2.175 \end{cases} \tag{25}$$

Notice in the above relation that adopting $C^+ = 5$ yields the starting point of the extended logarithmic layer for flow over smooth walls as $y_l^+ \cong 7.2$.

5.4 Existing description of the core layer

To arrive at the velocity distribution in the core layer, Eq. (4) combined with Eqs. (6) or (7) must be solved, depending on the flow configuration. In these equations, the dimensionless eddy viscosity needs to be obtained from a turbulence model, which must satisfy the following criteria [7]:

$$\frac{d}{d\eta}\left(\frac{\upsilon_t}{\upsilon}\right)\Big|_{\eta=0} = 0 \tag{26}$$

$$\frac{d}{d\eta}\left(\frac{\upsilon_t}{\upsilon}\right)\Big|_{\eta\to 1} = -\kappa Re_\tau \tag{27}$$

The solution of the core layer strongly depends on the flow geometry. Table 2 summarizes the turbulence models employed according to the existing description of the core layer as well as the obtained velocity profiles for the current benchmark problems. It should be mentioned that for the turbulent boundary layer flow over a flat plate, since we are interested to provide an analytic solution, the approximate von Karman profile for the shear stress of the laminar case is adopted here.

In each of the problems presented in Table 2, the following parameter is used to analyze the level of consistency of the employed turbulence model with the experimental data:

$$\overline{C} = -\lim_{\eta\to 1}\int_0^\eta \left(\frac{du^+}{d\eta} + \frac{1}{\kappa(1-\eta)}\right)d\eta \tag{28}$$

This parameter demonstrates the discrepancies appearing between the values of the dimensionless eddy viscosity and (a) the linear relation of $\kappa Re_\tau(1-\eta)$ for the Couette flow (b) the parabolic relation $\kappa Re_\tau\eta(1-\eta)$ for the channel flow, the

Table 2 The utilized turbulence models in conjunction with the existing core layer solutions for the current benchmark problems

Geometry	Range of η	$\frac{\upsilon_t}{\upsilon}(\eta)$	$u_c^+ - u^+$	Obtained $\overline{C}$
Couette flow	$-1 < \eta < 1$	$\frac{\kappa Re_\tau}{26}(1-\eta^2)(12+\eta^2)$	$\frac{1}{\kappa}ln\frac{1+\eta}{1-\eta} + \frac{\eta}{6\kappa}$	2.1
Channel flow	$-1 < \eta < 1$	$\frac{\kappa Re_\tau}{6}(1-\eta^2)(1+2\eta^2)^*$	$\frac{1}{\kappa}ln\frac{1+2\eta^2}{1-\eta^2}$	1.0
Pipe flow	$0 < \eta < 1$	$\frac{\kappa Re_\tau}{6}(1-\eta^2)(1+2\eta^2)^*$	$\frac{1}{\kappa}ln\frac{1+2\eta^2}{1-\eta^2}$	1.0
Flat plate	$0 \leq \eta < 1$	$\frac{\kappa Re_\tau}{12}(1-\eta^2)(1+5\eta^2)$	$\frac{1}{\kappa}ln\frac{1+5\eta^2}{1-\eta^2}$	2.7

*These turbulence models are taken from the book of Gersten and Herwig [34]. However, the relations for the Couette flow as well as flow over a flat plate are proposed here in a way that the resulting $\overline{C}$'s fit well with their suitable values

pipe flow, and flow over a flat plate. The value of $\overline{C}$ should be ≅ 2.1 for the Couette flow, ≅ 1 for the channel and pipe flows, and ≅ 2.7 for the flow over a flat plate, as suggested in [7].

The constant $u_c^+ = u^+(\eta = 0)$ appearing in Table 2 represents the dimensionless velocity at the centerline of the Couette flow as well as the channel and pipe flows while it stands for the dimensionless velocity at the edge of the boundary layer (i.e., free stream velocity) for flow over the flat plate. This parameter is defined as [7]:

$$u_c^+ = \frac{1}{\kappa}\mathrm{Ln}\,\mathrm{Re}_\tau + C^+ + \overline{C} \tag{29}$$

5.5 The proposed description for the core layer

The existing relations for the core layer lose their accuracy in the vicinity of the wall. However, in this section, a new description for the core layer (the extended core layer) is proposed in a way that the range of applicability of this layer enhances substantially. In this description, provided that $y_l^+ > 0$, the core layer solution remains accurate until the viscous sublayer in a way that even the extended logarithmic layer is omitted completely. Meanwhile, for $y_l^+ \le 0$ (wherein the viscous sublayer vanishes), the extended core layer encompasses the entire flow field. With this contribution, we arrive at a two-layer description for the current benchmark problems.

As mentioned in Sect. 5.4, at the start of the core layer (i.e., $\eta \to 1$), the dimensionless eddy viscosity alter linearly according to Eq. (27). In the description proposed here, we change the position wherein the linear variation of the dimensionless eddy viscosity initiates. Indeed, this point is transferred from the wall to the ending point of the viscous sublayer. To this aim, a new variable is introduced for the dimensionless distance as $z = \eta/\eta_l$. With this definition, provided that $y_l^+ > 0$, $z = 1$ instead of referring to the wall position, represents the ending point of the viscous sublayer. Meanwhile, for $y_l^+ \le 0$, $z = 1/\eta_l$ refers to the wall. The change of variable results in:

$$\frac{\mathrm{d}\left(\upsilon_t/\upsilon\right)}{\mathrm{d}z} = \eta_l \frac{\mathrm{d}\left(\upsilon_t/\upsilon\right)}{\mathrm{d}\eta} \tag{30}$$

Hence, according to Eq. (27), one has:

$$\left.\frac{\mathrm{d}\left(\upsilon_t/\upsilon\right)}{\mathrm{d}z}\right|_{z=1} = -\kappa \mathrm{Re}_\tau \eta_l \tag{31}$$

Table 3 presents the proposed turbulence models in conjunction with the corresponding core layer solutions for the current benchmark problems.

The constants coefficients appearing in Table 3 are:

$$A = \sqrt{1+\frac{8}{13}\varepsilon},\ B = \sqrt{\frac{13}{2}A - \frac{11}{2}},\ C = \sqrt{1+\frac{16}{3}\varepsilon},\\ D = \sqrt{1+\frac{20}{3}\varepsilon},\ \varepsilon = \frac{1}{\kappa \mathrm{Re}_\tau \eta_l} \tag{32}$$

Meanwhile, u_l^+ is defined here as:

$$u_l^+ = u^+\left(\eta = \eta_l\right) = u^+(z = 1) \tag{33}$$

For small values of the wall roughness wherein the viscous sublayer establishes (i.e.,$y_l^+ > 0$), one has:

$$u_l^+ = \mathrm{Re}_\tau\left(1 - \eta_l\right) = y_l^+ \tag{34}$$

However, in the absence of the viscous sublayer occurring at the high values of the wall roughness (i.e.,$y_l^+ < 0$), u_l^+ must be obtained from the above equations in a way that the velocity at the wall vanishes.

5.5.1 Simplifying the extended core layer for high Re numbers

At the high values of the Reynolds number, the constant coefficients appearing in Eq. (32) reduce to:

Table 3 The proposed turbulence models in conjunction with the extended core layer solutions for the current benchmark problems

Geometry	Range of z for $\eta_l \le 1$*	$\frac{\upsilon_t}{\upsilon}(z)$	$u^+ - u_l^+$
Couette flow	$-1 \le z \le 1$	$\frac{\kappa Re_\tau \eta_l}{26}\left(1-z^2\right)\left(12+z^2\right)$	$\frac{1}{\kappa A}\left[\frac{1}{B} ln \frac{(B-z)(B+1)}{(B+z)(B-1)} + \frac{4(1-z)}{13A+11}\right]$
Channel flow	$-1 \le z \le 1$	$\frac{\kappa Re_\tau \eta_l}{6}\left(1-z^2\right)\left(1+2z^2\right)$	$\frac{\eta_l}{\kappa C} ln\left[\frac{(1+3C-4z^2)}{(4z^2+3C-1)}\frac{(C+1)}{(C-1)}\right]$
Pipe flow	$0 \le z \le 1$	$\frac{\kappa Re_\tau \eta_l}{6}\left(1-z^2\right)\left(1+2z^2\right)$	$\frac{\eta_l}{\kappa C} ln\left[\frac{(1+3C-4z^2)}{(4z^2+3C-1)}\frac{(C+1)}{(C-1)}\right]$
Flat plate	$0 \le z \le 1$	$\frac{\kappa Re_\tau \eta_l}{12}(1-z^2)\left(1+5z^2\right)$	$\frac{\eta_l}{\kappa D} ln\left[\frac{(2+3D-5z^2)(D+1)}{(5z^2+3D-2)(D-1)}\right]$

* For $\eta_l > 1$, the range of applicability of the description is altered to $-1/\eta_l \le z \le 1/\eta_l$ for the Couette flow and the channel flow and $0 \le z \le 1/\eta_l$ for the pipe flow and the flat plate

$$A \cong 1+\frac{4}{13}\varepsilon, B \cong 1+\varepsilon, C \cong 1+\frac{8}{3}\varepsilon, D \cong 1+\frac{10}{3}\varepsilon \quad (35)$$

This alters the proposed velocity profiles of Table 3 to those reported in Table 4. These velocity profiles bear a strong resemblance to those of Table 2. The discrepancy goes back to the existence of ε, which is a small parameter. Notice that at the limiting case of $Re_\tau \to \infty$, provided that $z \neq \pm 1$, one has $\varepsilon \cong 0$, which reduces the proposed velocity profiles in Table 4 to those of the existing ones, reported in Table 2. Unlike the existing velocity profiles for the core layer, which approach to infinity at $\eta = \pm 1$, the proposed profiles remain bounded at $z = \pm 1$. Thus, they provide well-posed solutions.

5.5.2 The suitability's of the extended core layer

The following points discuss the suitability of the proposed core layer solutions:

Suitability # 1: Unlike the existing relations, in the proposed description, the velocity magnitude remains bounded at $z \to \pm 1$ for the whole ranges of the Reynolds number in the turbulent flow regime. More precisely, at $z = 1$ for all of the current configurations, one has: $u^+ = u_l^+$, which is the velocity at the ending point of the viscous sublayer. Meanwhile, at $z = -1$, the relation of $u^+ = u_l^+$ is recovered for the channel flow, while for the Couette flow, one has $u^+ = 2u_c^+ - u_l^+ = u_{wall}^+ - u_l^+$.

Suitability # 2: The following limit clearly shows that the velocity profile of the extended core layer automatically converts into the velocity profile of the extended logarithmic layer, (i.e. Equation (19)) as:

$$\lim_{z\to 1 \& \mathrm{Re}_\tau \to \infty} u^+ = C^+ + \frac{1}{\kappa}\ln\left(y^+ - y_l^+ + \frac{1}{\kappa}\right) \quad (36)$$

This successfully proves that with the proposed description, the need to incorporate the extended logarithmic layer (which itself includes the buffer layer and the logarithmic layer) is removed. Hence, with this description, only two layers including the viscous sublayer and the extended core layer suffice for the analysis. When the Reynolds number is sufficiently large, the laminar sublayer become so small that can be easily ignored. This confines the attention only to the extended core layer.

Suitability # 3: When $Re \to 0$ (i.e., $\mathrm{Re} < \mathrm{Re}_{crit}$), the laminar flow regime prevails and the viscous sublayer covers the entire flow field. In this limiting case, one has: $\eta_l = 0$. Hence:

$$u^+ = \begin{cases} \mathrm{Re}_\tau(1-\eta) & -1 \le \eta \le 1 \ \text{Couette flow} \\ \frac{1}{2}\mathrm{Re}_\tau(1-\eta^2) & -1 \le \eta \le 1 \ \text{Channel flow} \\ \frac{1}{2}\mathrm{Re}_\tau(1-\eta^2) & 0 \le \eta \le 1 \ \text{Pipe flow and flowover a flat plate} \end{cases} \quad (37)$$

Hence, one may concluded that the current two-layer description is applicable to the arbitrary value of the Reynolds number.

5.6 Further validation of the proposed two-layer description

Finally, in this section, the proposed two-layer description is utilized to simulate the flow field in the current benchmark problems. At the same time, the obtained results are compared with those of the open literature to validate this description further.

In Fig. 6, the obtained results in terms of the velocity profile in the Couette flow are compared with the experimental evidences of Reichardt from the book of Schlichting [33]. The presented results correspond to different values of the Reynolds numbers including $\mathrm{Re} = 2900, 34000$. Here, results of $Re = 1200$ belonging to the laminar flow regime is also provided to explore the suitability of the proposed description in the prediction of laminar flow fields. Obviously, the predicted results closely obey the experimental data.

Figure 7 compares the variations of the turbulent shear stress and the total shear stress in the channel flow with the experimental results of Reichardt from the book of Schlichting [33]. It is evident that $\tau_{total}/\overline{\tau}_w$ varies linearly within the whole channel. Scrutiny of $\tau_t/\overline{\tau}_w$, however, demonstrates

Table 4 Solutions for the extended core layer of the current benchmark problems at the high values of the Reynolds numbers

Geometry	Range of z for $\eta_l \le 1$*	$u_c^+ - u^+(z)$	u_c^+
Couette flow	$-1 \le z \le 1$	$\frac{1}{\kappa}\left[\ln\frac{(1+\varepsilon+z)}{(1+\varepsilon-z)} + \frac{z}{6}\right]$	$\frac{1}{\kappa}\left[\ln Re_\tau + \ln 2\kappa\eta_l + \frac{1}{6}\right]$
Channel flow	$-1 \le z \le 1$	$\frac{\eta_l}{\kappa}\ln\left[\frac{2z^2+1}{1+2\varepsilon-z^2}\right]$	$\frac{\eta_l}{\kappa}\left[\ln Re_\tau + \ln\frac{3\kappa\eta_l}{2}\right]$
Pipe flow	$0 \le z \le 1$	$\frac{\eta_l}{\kappa}\ln\left[\frac{2z^2+1}{1+2\varepsilon-z^2}\right]$	$\frac{\eta_l}{\kappa}\left[\ln Re_\tau + \ln\frac{3\kappa\eta_l}{2}\right]$
Flat plate	$0 \le z \le 1$	$\frac{\eta_l}{\kappa}\left[\ln\frac{5z^2+1}{1+2\varepsilon-z^2}\right]$	$\frac{\eta_l}{\kappa}\left[\ln Re_\tau + \ln 3\kappa\eta_l\right]$

* For $\eta_l > 1$, the range of applicability of the results is similar to Table 3

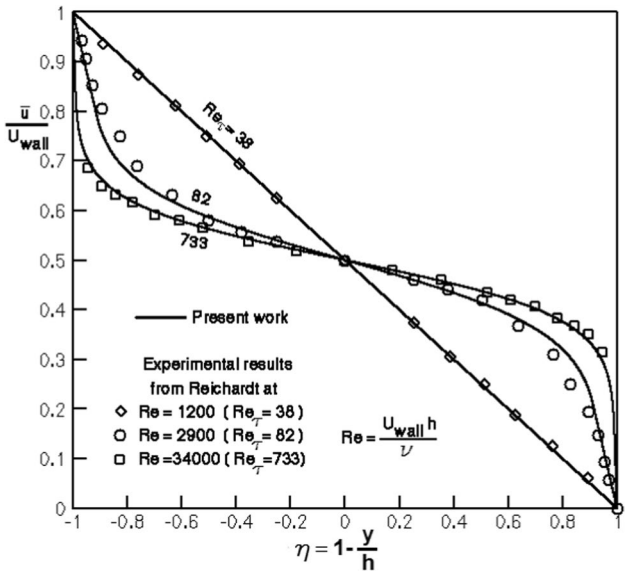

Fig. 6 Velocity profile in the Couette flow compared with the experimental results of Reichardt from the book of Schlichting [33] under different Reynolds numbers (At $Re = 2900, 34000$ the flow is turbulent while at $Re = 1200$ the flow is laminar)

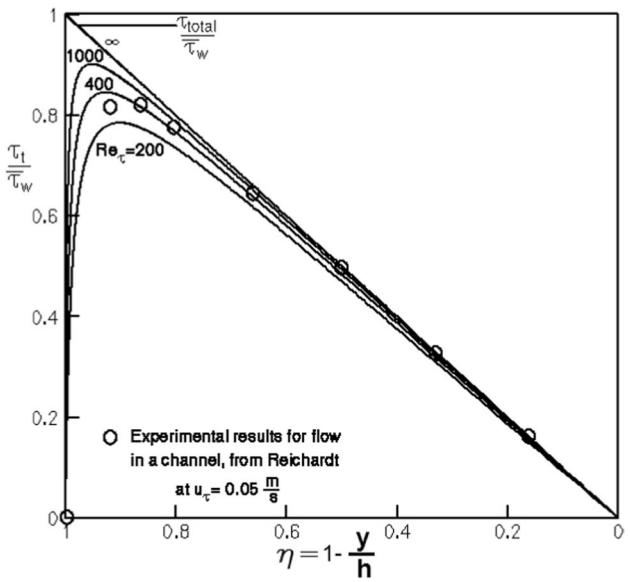

Fig. 7 Variations of the turbulent shear stress and the total shear stress in the channel flow compared with the experimental results of Reichardt from the book of Schlichting [33]

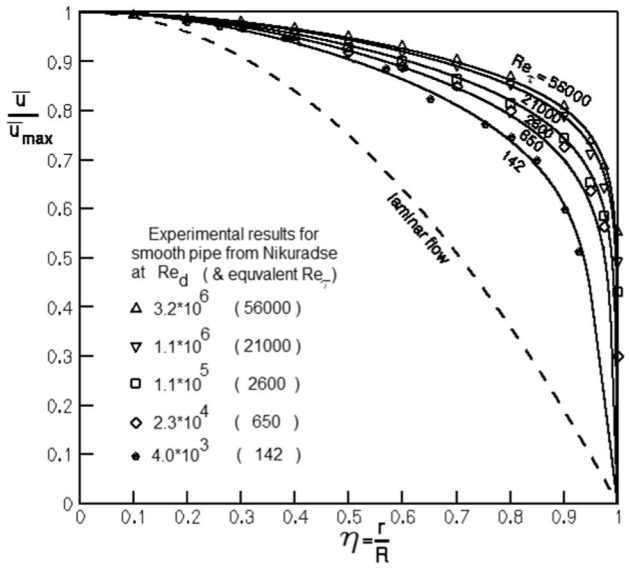

Fig. 8 Velocity profile in a smooth pipe compared with the experimental evidences of Nikuradse from the book of Schlichting [33]

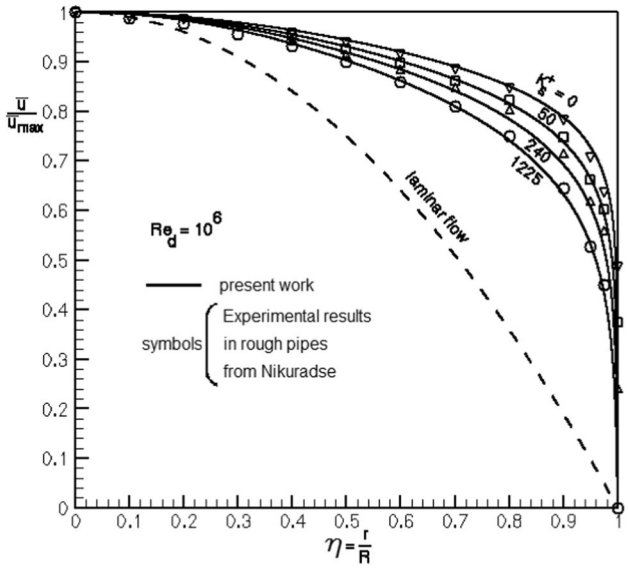

Fig. 9 Velocity profile in a pipe flow with a rough wall compared with the experimental evidences of Nikuradse from the book of Schlichting [33]

that this parameter follows the trend of $\tau_{\text{total}}/\overline{\tau}_w$ within the most parts of the channel. Meanwhile, in the vicinity of the wall, the trend is altered and $\tau_t/\overline{\tau}_w$ approaches to zero. Notice that the experimental results of Reichardt verifies the accuracy of the proposed description.

In Figs. 8 and 9, velocity profiles at different values of the Reynolds number ($Re_d = 2\overline{u}_m R/\upsilon$) are compared with the experimental evidences of Nikuradse from the book of Schlichting [33], which correspond to the smooth and rough pipes, respectively. In both of the figures, the parabolic profile of the laminar flow is also provided for comparison. Notice the close agreement between the presented results,

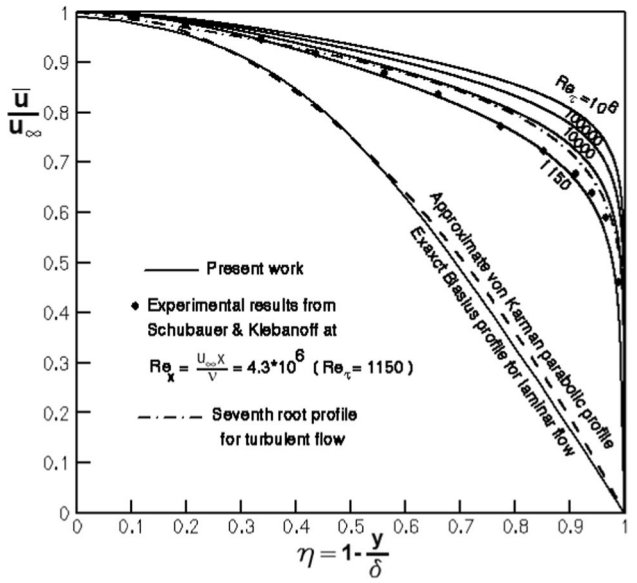

Fig. 10 Velocity profile over a flat plate at $Re_x = 4.3 \times 10^6$ compared with the experimental results of Schubauer and Klebanoff from the book of Schlichting and Gersten [7]

which again explore the suitability of the proposed two-layer description.

Finally, velocity profile over a flat plate at $Re_x = 4.3 \times 10^6$ is compared with the experimental results of Schubauer and Klebanoff from the book of Schlichting and Gersten [7] in Fig. 10. Here, the approximate von Karman parabolic profile and the exact Blasius profile belonging to the laminar flow as well as the seventh root profile for the turbulent flow are also plotted for comparison. This figure again verifies the accuracy of the proposed description.

6 Concluding remarks

In this work, we discussed the basic relation of:

$$\frac{\mathrm{d}u^+}{\mathrm{d}y^+} = \frac{1}{1+\frac{\upsilon_t}{\upsilon}(y^+)} \frac{\tau_{\text{total}}\left(y^+\right)}{\overline{\tau}_w} \tag{38}$$

for the Couette flow, the 2D channel flow, the circular pipe flow, and flow over a flat plate, which are four benchmark problems in fluid mechanics. This relation is exact and applicable to the entire flow field. However, it was discussed that some improper use of this relation has been occurred, which reduced the accuracy of the existing theory of turbulent flows and led to a four-layer description for these turbulent flow fields. The shortcomings and the utilized strategies to remove them are summarized below:

1) In the existing theory, the linear relation of $\upsilon_t/\upsilon = \kappa y^+$ has improperly been utilized for the near-wall layer. This assumption may not hold in the low values of y^+ and necessitates to consider an additional layer (i.e., the buffer layer) to capture the flow field between the viscous sublayer and the logarithmic layer. To remove this shortcoming, in this work, the relation of $\upsilon_t/\upsilon = \kappa\left(y^+ - y_l^+\right)$ was proposed. This relation extended the logarithmic layer up to the viscous sublayer and excluded the need to incorporate the buffer layer as a distinct layer with its complex formula. More specifically, in the special case of flow over smooth walls, we arrived to the following relations for the near-wall layer:

$$\frac{\upsilon_t}{\upsilon} = \begin{cases} 0 & \text{for} y^+ \le 7.2 \\ \kappa y^+ - 3 & \text{for } y^+ \ge 7.2 \end{cases} \tag{39}$$

$$\frac{\mathrm{d}u^+}{\mathrm{d}y^+} = \begin{cases} 1 & \text{for } y^+ \le 7.2 \\ \frac{1}{\kappa y^+ - 2} & \text{for } \ge 7.2 \end{cases} \tag{40}$$

$$u^+ = \begin{cases} y^+ & \text{for} y^+ \le 7.2 \\ 5 + \frac{1}{\kappa}\ln\left(y^+ - 5\right) & \text{for } y^+ \ge 7.2 \end{cases} \tag{41}$$

2) In the existing theories, it is improperly assumed that $\upsilon_t \gg \upsilon$ in the logarithmic layer as well as the core layer, which may not hold in the low values of the Reynolds number or in the vicinity of the wall. It was shown that avoiding this improper assumption substantially enhanced the range of applicability of the obtained velocity profile for logarithmic layer as well as the core layer.

3) In the proposed theory, a new variable was introduced for the dimensionless distance in the analysis of the core layer. With the aid of this variable, we changed the position wherein the core layer initiated. Indeed, this point was transferred from the wall to the ending point of the viscous sublayer. This contribution enhanced the range of applicability of the core layer substantially. Hence, we arrived at a two-layer description for the current benchmark problems, which included only the viscous sublayer and the extended core layer.

The work presented here aimed to clarify the analysis of some benchmark turbulent flows and make it more accessible to students who are studying fluid mechanics for the first time.

Author contributions SRS contributed to conceptualization, methodology, and writing–original draft preparation; IZ done formal analysis and investigation, writing–review and editing.

Funding This research received no specific grant from any funding agency, commercial or not for profit sectors.

Declarations

Conflict of interest The authors have no conflicts of interests to disclose.

References

1. Saleh R, Rahimi AB (2004) Axisymmetric stagnation-point flow and heat transfer of a viscous fluid on a moving cylinder with time-dependent axial velocity and uniform transpiration. J Fluids Eng 126:997–1005. https://doi.org/10.1115/1.1845556
2. Ghiasi EK, Saleh R (2018) Unsteady shrinking embedded horizontal sheet subjected to inclined Lorentz force and Joule heating, an analytical solution. Results Phys 11:65–71. https://doi.org/10.1016/j.rinp.2018.07.026
3. Housiadas KD, Georgiou GC (2018) Analytical solution of the flow of a Newtonian fluid with pressure-dependent viscosity in a rectangular duct. Appl Math Comput 322:123–128. https://doi.org/10.1016/j.amc.2017.11.029
4. Kannaiyan A, Varathalingarajah T, Natarajan S (2021) Analytical solutions for the incompressible laminar pipe flow rapidly subjected to the arbitrary change in the flow rate. Phys Fluids 33:043601. https://doi.org/10.1063/5.0043519
5. Akhtar S, Shah NA (2018) Exact solutions for some unsteady flows of a couple stress fluid between parallel plates. Ain Shams Eng J 9:985–992. https://doi.org/10.1016/j.asej.2016.05.008
6. Nec Y, Huculak G (2020) Exact solutions to steady radial flow in a porous medium with variable permeability. Phys Fluids 32:077108. https://doi.org/10.1063/5.0014476
7. Schlichting H, Gersten K (2016) Boundary-layer theory. Springer, Berlin Heidelberg
8. White FM (2010) Fluid Mechanics. 7th ed. McGraw-Hill.
9. García FJG, Alvariño PF (2019) On an analytic solution for general unsteady/transient turbulent pipe flow and starting turbulent flow. Euro J Mech - B/Fluids 74:200–210. https://doi.org/10.1016/j.euromechflu.2018.11.014
10. Hasan MK, Manasseh R, Leontini JS (2019) Analytic representations of dissipation in partially-submerged reciprocating pipe flow. Euro J Mech - B/Fluids 75:97–104. https://doi.org/10.1016/j.euromechflu.2018.12.006
11. Heinz S (2018) On mean flow universality of turbulent wall flows. I. High Reynolds number flow analysis. J Turbul 19:929–958. https://doi.org/10.1080/14685248.2019.1566736
12. Kadivar M, Tormey D, McGranaghan G (2021) A review on turbulent flow over rough surfaces: Fundamentals and theories. Int J Thermofluids 10:100077. https://doi.org/10.1016/j.ijft.2021.100077
13. Teja KM, Narasimhamurthy VD, Andersson HI, Pettersen B (2021) Onset of shear-layer instability at the interface of parallel Couette flows. Int J Heat Fluid Flow 89:108786. https://doi.org/10.1016/j.ijheatfluidflow.2021.108786
14. Ohta T, Osaka F, Kitagawa Y (2022) Modulation of turbulent Couette flow with vortex cavitation in a minimal flow unit. J Turbul 23:152–172. https://doi.org/10.1080/14685248.2022.2046762
15. Hasanuzzaman G, Merbold S, Motuz V, Egbers C (2022) Enhanced outer peaks in turbulent boundary layer using uniform blowing at moderate Reynolds number. J Turbul 23:68–95. https://doi.org/10.1080/14685248.2021.2014058
16. Jiao Y, Chernyshenko S, Hwang Y (2022) A driving mechanism of near-wall turbulence subject to adverse pressure gradient in a plane Couette flow. J Fluid Mech. https://doi.org/10.1017/jfm.2022.300
17. İlter YK, Çetinkaya A, Ünal UO (2023) Large eddy simulations of the turbulent channel flow over dimpled surfaces. J Turbul 24:2186415. https://doi.org/10.1080/14685248.2023.2186415
18. Mangavelli SC, Yuan J, Brereton GJ (2021) Effects of surface roughness topography in transient channel flows. J Turbul 22:434–460. https://doi.org/10.1080/14685248.2021.1927057
19. Kracik J, Dvorak V (2023) Effect of wall roughness on secondary flow choking in supersonic air ejector with adjustable motive nozzle. Int J Heat Fluid Flow 103:109168. https://doi.org/10.1016/j.ijheatfluidflow.2023.109168
20. Li M, de Silva CM, Chung D, Pullin DI, Marusic I, Hutchins N (2022) Modelling the downstream development of a turbulent boundary layer following a step change of roughness. J Fluid Mech. 22:731. https://doi.org/10.1017/jfm.2022.731
21. Sorgun M, Ulker E, Uysal SOK, Muftuoglu TD (2022) CFD modeling of turbulent flow for non-newtonian fluids in rough pipes. Ocean Eng 247:110777. https://doi.org/10.1016/j.oceaneng.2022.110777
22. Aghaei-Jouybari M, Yuan J, Li Z, Brereton GJ, Jaberi FA (2022) Supersonic turbulent flows over sinusoidal rough walls. J Fluid Mech. https://doi.org/10.1017/jfm.2022.1049
23. Hosseinzade H, Bergstrom DJ (2023) A wall stress model to predict high-Reynolds number flow over rough walls. Int J Heat Fluid Flow 100:109116. https://doi.org/10.1016/j.ijheatfluidflow.2023.109116
24. She ZS, Chen X, Hussain F (2017) Quantifying wall turbulence via a symmetry approach: a Lie group theory. J Fluid Mech 827:322–356. https://doi.org/10.1017/jfm.2017.464
25. White FM (1991) Viscous Fluid Flow. 2nd ed. McGraw-Hill.
26. Durbin PA (2023) Reflections on roughness modelling in turbulent flow. J Turbul 24:3–13. https://doi.org/10.1080/14685248.2022.2137171
27. Ismail U (2023) Direct numerical simulation of a turbulent boundary layer encountering a smooth-to-rough step change. Energies 16:1709. https://doi.org/10.3390/en16041709
28. Squire D, Morrill-Winter C, Hutchins N, Schultz M, Klewicki J, Marusic I (2016) Comparison of turbulent boundary layers over smooth and rough surfaces up to high Reynolds numbers. J Fluid Mech 795:210–240. https://doi.org/10.1017/jfm.2016.196
29. Tani I (1987) Turbulent Boundary Layer Development over Rough Surfaces. In Perspectives in Turbulence Studies. Berlin, Heidelberg: Springer Berlin Heidelberg.
30. Colebrook CF (1939) Turbulent flow in pipes, with particular reference to the transition region between the smooth and rough pipe laws. J Inst Civil Eng 11:133–156. https://doi.org/10.1680/ijoti.1939.13150
31. Mckeon BJ, Morrison JF, Jiang W, Li J, Smits AJ (2003) Revised log-law constants for fully-developed turbulent pipe flow, in IUTAM symposium on Reynolds number scaling in turbulent flow, A.J. Smits, Editor., Kluwer Academic Publishers: Dordrecht.
32. Merzkirch W, ed. Fluid Mechanics of Flow Metering. 2004, Springer-Verlag.
33. Schilichting H (1978) Boundary Layer Theory. 7th ed. McGraw-Hill.
34. Gersten K, Herwig H (1994) Strömungsmechanik Grundlagen der Impuls-, Warme- und Stoffübertragung aus asymptotischer Sicht. Vieweg-Verlag, London
35. Kestin J, Richardson PD (1963) Heat transfer across turbulent, incompressible boundary layers. Int J Heat Mass Transf 6:147–189. https://doi.org/10.1016/0017-9310(63)90035-8